



Etching of blood proteins in the early and late flowing afterglow of oxygen plasma

Journal:	<i>Plasma Processes and Polymers</i>
Manuscript ID:	ppap.201300067.R2
Wiley - Manuscript type:	Full Paper
Date Submitted by the Author:	n/a
Complete List of Authors:	Vesel, Alenka; Jozef Stefan Institute, Plasma laboratory Kolar, Metod; Jozef Stefan International Postgraduate School, Recek, Nina; Jozef Stefan International Postgraduate School, Kutasi, Kinga; Institute for Solid State Physics and Optics, Stana-Kleinschek, Karin; Faculty of Mechanical Engineering, University of Maribor, Laboratory for Characterization and Processing of Polymers Mozetic, Miran; Jozef Stefan Institute,
Keywords:	

SCHOLARONE™
Manuscripts

Review

((please add journal code and manuscript number, e.g., DOI: 10.1002/ppap.201100001))

Article type: Full Paper

Etching of blood proteins in the early and late flowing afterglow of oxygen plasma

Alenka Vesel*, Metod Kolar, Nina Recek, Kinga Kutasi, Karin Stana-Kleinschek, Miran Mozetic

Dr. A. Vesel, Prof. M. Mozetic

Plasma laboratory, Jozef Stefan Institute, Jamova cesta 39, 1000 Ljubljana, Slovenia

E-mail: alenka.vesel@guest.arnes.si

M. Kolar, N. Recek

Jozef Stefan International Postgraduate School, Jamova cesta 39, 1000 Ljubljana, Slovenia

Prof. K. Stana-Kleinschek

Laboratory for Characterization and Processing of Polymers, Faculty of Mechanical Engineering, University of Maribor, Smetanova 17, 2000 Maribor, Slovenia

Dr. K. Kutasi

Institute for Solid State Physics and Optics, Wigner Research Centre for Physics, Hungarian Academy of Sciences, POB 49, H-1525 Budapest, Hungary

Abstract

Films of proteins fibrinogen and albumin are exposed to neutral reactive particles in order to study their etching rates in early and late oxygen afterglows of microwave plasma. The etching rates are determined at different pressures between 50 and 400 Pa. The etching rates for both proteins first increase with the increasing pressure, while later they reach a constant value. Furthermore, the etching rates are higher in the early than in the late afterglow. The concentration of all available species in the afterglow, i.e. neutral oxygen atoms in the ground state, neutral molecules in the first excited state and ozone is determined either by experimental measurements or theoretically using a well-established model. The etching rates are explained by the synergistic effects of atoms and metastable molecules.

Introduction

Low-pressure non-equilibrium gaseous plasmas have been used for cleaning and decontamination of various materials for decades. The technique exhibits enormous potential for applications in medicine, where the needs for the development of efficient sterilization and decontamination techniques are extremely high. A decade ago a survey on hospital-acquired infections in the United States showed over 2 million cases each year and it is estimated to cause almost 100,000 deaths per year.^[1] Lipscomb et al. performed extensive work on contamination of 260 “sterile” medical instruments obtained anonymously from nine primary care trusts. A high level of proteinaceous soiling was found on many of the tested instruments.^[1] A lot of work has already been performed on the sterilization of surgical instruments,^[2-7] while much less work has been performed on the removal of various pathogenic biomolecules such as bacterial endotoxins or prion proteins.^[8-12] The presence of endotoxins in the blood (endotoxemia) can lead to septic shock, while prion proteins can cause severe neurodegenerative diseases such as Creutzfeldt–Jakob disease. Therefore, special care has to be taken for assuring the sufficient cleanliness of surgical instruments. Pathogenic residues that can be present on the surface of surgical instruments are quite resistant towards classical cleaning methods such as thermal treatment (autoclaves), chemical treatment or ionizing radiation.^[13] This is a reason for seeking alternative cleaning methods, and one of the most promising methods is plasma treatment. Fricke et al. used selected polymers as model materials simulating bacterial cells and performed extensive research on removal of such materials.^[14] They used atmospheric plasma jets and found huge etching rates of the order of 100 nm/s depending on the polymeric material. They concluded that such treatment could be used for removal of organic materials including microorganisms from surfaces.^[14-15] Due to the small dimensions of the jet strong radial dependences as well as longitudinal dependences were observed.

Plasma has many advantages when compared with classical methods. It is non-toxic and it is maintained at low temperatures, thus being useful for treating heat-sensitive materials. Plasma readily reacts with organic materials and can cause extensive etching/removal of surface material. But as reported by Kylian et al., the required conditions leading to the inactivation of bacteria or the removal of biological residues are different.^[5] In the case of bacteria sterilization, the synergistic effects of UV photons and chemically active species are important, so an optimal ratio of UV photons and a concentration of reactive plasma species is beneficial. UV photons cause damage to genetic material, while chemically active species can damage spore and bacterial walls by etching. It was found that for bacteria sterilization extensive UV radiation is desirable, while in the case of the removal of pathogenic molecules a maximum concentration of active species is necessary. This is not the only reason that complicates the plasma cleaning procedure. The removal of biomolecules from medical instruments by plasma could also be a difficult task due to the fact that many medical instruments are made of polymer materials, which can be etched in plasma as well. Therefore, special care should be taken when choosing the right plasma parameters for the removal of proteins while leaving the polymer surface of the medical instruments intact. The exact mechanism of plasma etching is still not clear due to a combination of various active species that are present in plasma. Experimental studies have shown that plasma etching can be very selective.^[16,17] As reported by Belmonte et al., species such as oxygen molecules in excited states, in particular $O_2(a)$, can have a synergistic effect in combination with neutral O-atoms.^[18-20]

In the present paper we report recent results on the interaction of reactive radicals created in gaseous plasma with model proteins. The blood proteins fibrinogen and human serum albumin were used. They were etched either in the early or late afterglow of oxygen plasma in order to understand the role of different plasma radicals. The etching rates of both proteins

were determined and compared to the etching rate of polymer polyethylene terephthalate, which had been determined previously.^[21]

Experimental Section

Sample Preparation

Thin films of proteins were deposited on quartz crystals by means of the spin coating technique. A diameter of the quartz crystals was 8 mm. In this case, human serum albumin (HSA) and fibrinogen (FIB) from Sigma-Aldrich were dissolved in Milli-Q water (Millipore, USA) at a concentration of 10 g L⁻¹ and 5 g L⁻¹, respectively. 50 µl of the prepared solution of the protein was deposited onto a quartz crystal microbalance sensor, which had been activated previously in microwave oxygen plasma at 100 W for 5 seconds, and spin coated with a spinning speed of 1500 revolutions per minute (rpm) and an acceleration of 1000 rpm sec⁻¹ for 30 sec. The sensors were afterwards dried in an oven at 37 °C for 1 hour.

Afterglow Treatment

A schematic diagram of the experimental system for the etching of proteins in oxygen plasma afterglow is presented in Figure 1. The afterglow chamber is a borosilicate glass tube with an inner diameter of 36 mm and a length of 80 cm. Molecular oxygen was introduced into a narrow quartz tube with an inner diameter of 5 mm. The tube was mounted into a microwave (MW) cavity. The cavity was connected to a MW generator with an adjustable power of up to 300 W operating at a frequency of 2.45 GHz. In our experiments the power was set at 150 W. The metallic parts of the MW cavity were cooled with water, while the quartz tube itself was forced air cooled. Molecular oxygen dissociated to atoms as it passed through the MW discharge. An example of optical emission spectrum of glowing MW plasma showing a very high dissociation fraction is presented in Figure 2. A movable catalytic probe was mounted in

the afterglow chamber as shown in Figure 1 in order to measure the density of O-atoms in the afterglow. The operation principles of catalytic probes are described in detail in the literature.^[22-23] The density of O-atoms depends on the discharge power (which was fixed in our experiments) and oxygen pressure. The pressure was varied between 50 Pa and 400 Pa. The density of O-atoms decreased with the increasing pressure. Under such experimental conditions the density of O-atoms was between 2.5×10^{20} and $7 \times 10^{20} \text{ m}^{-3}$ for the case of late afterglow (LAG), and between 5×10^{20} and $13.5 \times 10^{20} \text{ m}^{-3}$ for the case of early afterglow (EAG) (Table 1). The position of EAG and LAG is shown in Figure 1. This is also the position where the samples were treated. In the case of a flowing system the “EAG” denotes the region that follows the discharge. Here the recombination of charged species starts. The end of “EAG”, i.e. the start of “LAG,” is defined at the position where the density of the charged species drops below the considerable limit. In our case the “EAG” started in the small diameter tube, where the discharge was also ignited. The afterglow chamber was pumped with a two-stage rotary pump operating at a nominal pumping speed of $80 \text{ m}^3 \text{ h}^{-1}$ and ultimate pressure below 1 Pa. Pressure in the system was measured with an absolute gauge covering the range of pressures between 1 and 1000 Pa. Since the system is hermetically tight, the ultimate pressure achieved after few minutes of pumping was below the detection limit of our gauge, i.e. 1 Pa. To be able to achieve higher pressures in the reactor flow rate needed to be increased from 140 sccm used to set 50 Pa to 2700 sccm in the case of 400 Pa. The length of the afterglow in the small diameter tube was about 6 cm depending on the conditions. At these gas flow rates the species flight time in this region is about 0.2 ms, during which the ion densities can decrease by two orders of magnitude.^[24] However, due to the expansion of the plasma afterwards in the larger diameter tube it resulted in a fast elapse of the ion densities. Thus the samples positioned in the jet direction at the bottom wall of the tube were exposed to the end of the “EAG” region, where the density of the charged species becomes negligible from the application point of view. Nevertheless, here the effect of the plasma jet, such as

high gas temperature and UV radiation, can be still accounted for. In comparison to “EAG” the “LAG” region is totally free of charged species and it is not in direct contact with the plasma jet.

Apart from charged particles and neutral oxygen atoms, other reactive particles are also created in oxygen plasma, as well as in the afterglow region. The most stable ones are neutral molecules in the first excited state $O_2(a)$, and ozone molecules. Our experimental system does not allow for measuring the densities of these reactive particles, therefore we have performed numerical calculations to determine the density distribution of all the species in the reactor. The discharge and early-afterglow regions have been described with the help of a kinetic model, while the evolution of neutral species in the afterglow reactor has been traced with a 3-D hydrodynamic model.^[24-26] The hydrodynamic model made possible the determination of the flow dynamics, as well as the density and temperature distributions in the large diameter tube (a detailed description of the system and the features revealed by modelling will be given in a future publication^[23]). The molecular kinetic scheme used in models contains all the relevant processes as presented in Ref. [25]. In the calculations the pressure drops along the small diameter tube and the length of the discharge, i.e. the flight time of species in the early afterglow developed in the small diameter tube has been taken into account. The gas temperature in the discharge region was taken at 500 K, while at the entrance of the large diameter tube it was assumed to be 450 K. The calculations have shown that due to the perpendicular injection of the plasma into the reactor, the temperature is close to room temperature in most parts of it, except for a 5 cm region around the inlet. Due to this temperature gradient a local minimum of the total density appears, which can be observed also in the species density distributions. According to this the maximum species densities do not occur in the jet axis, but shift towards a lower temperature position in the pumping outlet direction, as can be seen in the axial distribution of $O_2(a)$ and O_3 densities shown in Figure 3a and 3b, respectively. The values at the positions marked with LAG and EAG in Figure 3 are

added to Table 1. The values presented in Figure 3 are calculated for the case of an empty tube. The samples definitely cause some drain of the reactive particles, but no attempt was made to take this effect into account due to unknown reaction probabilities.

Samples of fibrinogen and albumin which were deposited onto Quartz Crystal Microbalance (QCM) sensors were treated either in EAG or LAG for different periods of time. The thickness of the protein film versus treatment time was determined by QCM in such a way that a sample was mounted into the chamber and exposed to the oxygen plasma afterglow, treated for a short period, mounted into the QCM to measure the thickness, mounted again into the chamber and so on. The procedure was repeated many times until the thickness of the protein film became immeasurable. Such treatment in rather short intervals of about 10 s allowed for negligible heating of the samples due to exothermic reactions that occur on surfaces upon oxidation. The surface of the samples was characterized before and after treatment by atomic force microscopy (AFM) and X-ray photoelectron spectroscopy (XPS).

AFM Measurements

An AFM (Solver PRO, NT-MDT, Russia) was used to characterize the topology of the samples. All measurements were performed in tapping mode using ATEC-NC-20 tips (Nano And More GmbH, Germany) with a resonance frequency of 210–490 kHz and a force constant of 12–110 Nm^{-1} . $2 \times 2 \mu\text{m}^2$ and $5 \times 5 \mu\text{m}^2$ AFM images were recorded on each sample.

XPS Characterization

An XPS characterization of protein films was performed in order to determine the chemical composition on the surfaces after deposition and after etching using an XPS device (TFA XPS Physical Electronics). The samples were excited with monochromatic Al $K_{\alpha 1,2}$ radiation at

1486.6 eV over an area of 400 μm^2 . Photoelectrons were detected with a hemispherical analyzer positioned at an angle of 45° with respect to the normal of the sample surface. XPS survey spectra were measured at a pass energy of 187 eV using an energy step of 0.4 eV, while high-resolution C1s spectra were measured at a pass energy of 23.5 eV using an energy step of 0.1 eV. An additional electron gun was used for surface neutralization during XPS measurements.

QCM Measurements

The thickness of the protein film *versus* plasma treatment time was determined by a QCM with a dissipation unit, QCM-D (Model E4, QSense AB, Göteborg, Sweden). The QCM measured the mass of the thin film deposited onto a quartz crystal sandwiched between two electrodes.^[28] The electrodes were connected to a power supply that caused the crystal to oscillate at its fundamental resonance frequency and several overtones. The resonance frequency is disturbed by the removal of a mass. In this way the removal rate of protein *versus* treatment time was measured. The thickness of the protein film was calculated from the change in frequency taking into account the estimated density of the deposited film, which was $1 \times 10^3 \text{ kg m}^{-3}$. The calculated thickness for some selected samples was compared with data obtained by ellipsometry. The values were the same within the limits of experimental error.

Results and Discussion

The removal of proteins during plasma treatment was monitored by a QCM, which is a common method for small mass measurements. In Figure 4 there is shown an example of the thickness of the protein layer *versus* etching time in early or late afterglows. From Figure 4 we can see that the thickness of the protein layer decreases with etching time. At the beginning the removal rate is faster, and later it slows down. Two other findings can be drawn

from Figure 4: (i) protein removal is faster in early afterglow in comparison to late afterglow and (ii) the removal of protein fibrinogen is much faster than the removal of albumin, although the latter is known to have a much smaller molecular mass (67 kDa for albumin against 340 kDa for fibrinogen).^[29,30]

The example shown in Figure 4 refers to the case when plasma was created at 50 Pa. For all other pressures we have observed a similar trend of protein removal; only the slope of the curves was different. The slope of the curve allowed for further calculations of the protein etching rate. In Figure 5 there is shown the maximum etching rate (calculated from the steepest part of the curve) of the proteins fibrinogen and albumin versus pressure. Again, the etching in early and late afterglows is compared. The etching rates were about 2.5-times and 3.5-times higher in the EAG than in the LAG for fibrinogen and albumin, respectively. From Figure 5 another important finding can be drawn: the etching rates for both proteins first increased with the increasing pressure, while later they reached a constant value. This unexpected behaviour will be discussed later.

In order to understand the observed differences in etching rates shown in Figure 4 and 5, XPS analyses were performed for albumin and fibrinogen during etching in EAG and LAG. The surface composition is shown in Table 2. For a better comparison, we also show the ratio of O/C and N/C in Figure 6. The surface of both proteins consists of carbon, oxygen, and nitrogen, as well as some sodium. In the case of albumin minor concentrations of sulphur and phosphorus are also found, while in the case of fibrinogen some chlorine is found on the surface. Na and Cl in fibrinogen are not in the same proportion, since original fibrinogen powder contained not just NaCl salt but also other salts like sodium citrate according to specification. After exposure to oxygen plasma the oxygen concentration increases, while the carbon concentration decreases, which is a sign of surface functionalization. Interestingly,

relative nitrogen concentration increases as well, which indicates that nitrogen is not etched at the same rate as carbon. This can be explained by the fact known from polymer surface functionalization, that nitrogen is not functionalized in plasma such as carbon, so there is no scission of bonds. Sodium concentration also increases after etching. Since it is inorganic it does not form volatile species with oxygen, and therefore it is probably not etched in the afterglow region. Here it is worth mentioning that our previous studies performed in glowing oxygen plasma showed strong sodium lines in optical emission spectra.^[31] Table 2 also shows that the surface composition does not change with increasing etching time (Figure 6). Furthermore, there is also no significant difference in surface composition when comparing EAG and LAG (Figure 6). So it seems that the surface is in all cases is saturated with oxygen atoms. The oxygen concentration is slightly higher on the surface of albumin than fibrinogen.

To gain better insight into the surface chemical changes that could be responsible for different etching rates, high-resolution carbon spectra C1s were recorded and compared. The result is shown in Figure 7. The spectra consist of three peaks typical for protein: the peak on the right belonging to C-C bonds, the middle one belonging to C-O(H) and C-NH₂ bonds and the left one belonging to O=C-NH₂ and O=C-OOH groups. From Figure 7 it is not possible to see any significant difference when comparing early and late afterglows. The albumin is slightly more oxidized than the fibrinogen (high intensity of the third left peak), which is in agreement with the higher oxygen concentration that was found in the case of albumin. But again, this does not explain the higher etching rate of fibrinogen in comparison to albumin.

To obtain additional information regarding the surface characteristics of plasma etched samples, AFM analyses were performed to reveal the surface topography which could influence the etching rates. The AFM images of the albumin and fibrinogen after etching in EAG and LAG are shown in Figure 8 and 9 respectively. Here we should mention that the

time-scale is not the same for both figures since albumin is etched at lower rate as fibrinogen. Some important differences can be observed when comparing Figure 8 and 9. The surface of the albumin in comparison to the fibrinogen is very smooth. After etching the albumin, the surface became nanorough, and it seems that roughness still increases with an increasing etching time. Again, no important differences can be observed when comparing EAG and LAG. In the case of the fibrinogen, some spikes or particles are observed on as-deposited sample. These features are also observed after etching, meaning that they were not removed. We suppose that they could be NaCl crystals since chlorine was found only in the case of fibrinogen and it originates from salts according to producer's specification (see also surface composition of as received protein powder in Table 2).

Finally, some XPS survey spectra were measured on samples treated for a very long time. Figure 10 represents 2 spectra: the lower curve was obtained on a virgin Au-coated quartz crystal and the upper curve is for a crystal coated with fibrinogen and treated in LAG for a very long time (2750 s). The high resolution gold peaks for both samples are represented in Figure 11.

Etching Mechanisms

The experimental results are summarized as follows: (i) both proteins are slowly etched when exposed to oxygen plasma afterglows; (ii) the surfaces are saturated with oxygen irrespective of treatment time; and (iii) the removal rate of deposited materials depends on treatment time. For the initial few tens of seconds, it can be approximated by a linear straight line. So, the etching rate could be determined. The etching rates are larger in the early afterglow than in the late afterglow. The etching rate is few times greater for fibrinogen than for albumin.

Let us discuss the observed results. The proteins will not be etched when exposed to an equilibrium oxygen atmosphere at room temperature. The observed results should be therefore explained by the interaction between the reactive oxygen species created in plasma.

Oxygen plasma contains a variety of reactive particles including positively and negatively charged molecules and also atoms, oxygen atoms in both ground and a variety of excited states, neutral molecules in excited states, and ozone molecules. Oxygen plasma is also a source of radiation in the wide range from the IR to the VUV region. Any explanation of interaction between reactive particles and organic material in plasma itself is almost impossible due to the great number of possible reactants. Oxygen plasma also causes extensive heating of samples. In order to simplify experimental conditions we chose afterglow instead of plasma. Thermal effects in the afterglow are often negligible due to the absence of highly energetic particles. In fact, only three types of reactive oxygen particles are found in the flowing afterglow at sufficiently-high concentrations: oxygen atoms in the ground state, O_2 molecules in the first excited state, which is metastable with a typical radiation time close to one hour, and O_3 molecules.

Let us first consider the interaction between ozone molecules and selected proteins. Ozone is known to cause the slow degradation of polymer materials even at room temperature. Therefore, it should also be an active oxidant for proteins. Figure 3b reveals the density of these molecules along the afterglow chamber at several pressures. Next to the exhaust from the narrow quartz tube the concentration is rather low, but increases with increasing distance from the exhaust. The production of ozone in the afterglow chamber is at three body collisions between atoms and molecules in the ground state ($O(^3P) + O_2(X,0) + O \rightarrow O_3 + O$).^[24-25] The major cause of ozone loss is at the collision with molecules in the second excited state ($O_2(b) + O_3 \rightarrow O_2(X) + O_2(X) + O(^3P)$).^[24-25] Since the density of $O_2(b)$ molecules decreases markedly along the afterglow tube, the quenching of O_3 decreases, while the O_3 production does not change significantly along the tube, which results in the increase of ozone density along the late afterglow. Interaction with ozone therefore cannot explain observed protein etching, since the effect is the opposite: proteins are etched much faster in the early than in late afterglow.

Another candidate for the etching of organic materials in oxygen plasma afterglows is the interaction with neutral atoms in the ground state $O(^3P)$. These radicals are fairly stable in the gas phase as long as the pressure is kept reasonably low as in our case. They are produced in gaseous plasma predominantly by the electron impact dissociation of parent molecules. The major mechanism of atomic oxygen loss at a low pressure is heterogeneous surface recombination. The recombination coefficient depends enormously on the type of material the afterglow chamber is made from, and is lowest for smooth glass surfaces; however, it can change due to the conditioning of the surface along the afterglow, resulting from the continuous use of the system, as well as due to the heating of the surface, e.g. at the plasma jet impact. The O atoms' density – measured by a catalytic probe – is found to be in the order of 10^{20} m^{-3} and to decrease monotonously along the afterglow chamber. The measurements show that at the early afterglow position the density is higher with a factor of 2 than that at the late afterglow position. Since the etching rate of proteins versus the position follows the same trend, the etching could be explained by sole interaction with the oxygen atoms. Unfortunately, the behaviour versus pressure is exactly the opposite: oxygen atom density decreases with increasing pressure (Table 1), but the etching of proteins definitely increases with increasing pressure. The etching thus cannot be explained by interaction with oxygen atoms only.

The last type of reactive particles which abound in oxygen plasma afterglows are molecules in the first excited state $O_2(a)$. Due to their low excitation energy (about 1 eV only) they are easily produced in oxygen plasma. These metastables have a very low recombination probability on a glass wall, i.e. 2×10^{-5} , therefore the major loss mechanism is gas phase relaxation by super-elastic collisions. As mentioned earlier, the probability for three body collisions in our range of pressures is very low, and that is why the density of $O_2(a)$ molecules in the afterglow chamber is of the order of 10^{21} m^{-3} . The density of these particles is therefore

great enough to result in protein etching. The density of such molecules in the EAG is only slightly higher than in the LAG, so the differences in etching rates between these two positions cannot be explained by these rather marginal differences in $O_2(a)$ density. Furthermore, the $O_2(a)$ density increases almost perfectly linearly with increasing pressure (Figure 3a and Table 1), while the etching rate of both proteins tends to become independent from pressure at high pressures (Figure 5). Here we should also note that, according to Silva et al., the $O_2(a)$ molecules can react alone with the aromatic rings.^[32] The proteins used in our experiments contain such rings but the concentration is rather small and they might be located in complex hindered structures, so any discussion on the exact mechanisms of interaction between $O_2(a)$ molecules and proteins is beyond the scope of this paper.

Dependences in the etching rate therefore cannot be explained by interaction with any of above mentioned reactive particles, so our experimental results indicate synergistic effects. Such effects have not been studied systematically by many authors. However, the recent work performed by Belmonte et al. is particularly worth mentioning.^[18-20] They performed a systematic treatment of selected polymers in oxygen plasma afterglows and found such synergies. Following this idea the polymer etching may well be a synergistic effect of the available particles. Since the behaviour of ozone density is completely different from polymer etching results, one can take into consideration the synergy of atoms and molecules in the first excited state. The product of both densities is shown in Figure 12. One can observe very similar behaviour as observed in Figure 5, so a possible explanation of the protein etching could be a synergy between atoms and excited molecules. Following the Belmonte's hypothesis the atoms cause the surface functionalization of proteins, and the modified material exhibits a high affinity for interaction with excited molecules. Chemical reactions following interaction with the said molecules cause intermediate oxides that decay to oxidation products such as CO_2 and H_2O , as well as more complex molecules.

Finally, it is worth mentioning that the degradation of proteins also occurs due to the absorption of VUV photons. Oxygen plasma is a source of photons arising from transitions of excited neutral oxygen atoms. The major resonance line is observed at 130.5 nm. According to Wertheimer et al., such photons cause the rapid degradation of polymers.^[33] The angular distribution of photons emitted from plasma is substantially uniform. The photon flux from the spot source decreases as $1/r^2$, where r is the distance from the source. Our plasma is not a spot source, but since the distance between the glowing plasma and the EAG position is much larger than the dimension of plasma inside the narrow tube, we can take into account such a rough approximation. According to Wertheimer oxygen plasma is a relatively poor source of VUV radiation as compared to hydrogen or nitrogen and taking into account the decrease of the intensity ($1/r^2$) of the effect of VUV radiation it is regarded as a minor cause of polymer degradation as compared to chemical reactions.

The evolution of protein morphology during the treatment is revealed from the AFM images and is summarized in Figure 8 and 9. A noticeable difference between albumin and fibrinogen is observed. While albumin forms a rather smooth film, some spikes are observed by the AFM in the case of fibrinogen. Furthermore, measurable quantities of sodium and chlorine are found on the surface of samples coated with fibrinogen (Table 2). The spikes could be explained by the specific conformation and agglomeration of fibrinogen, but a more reasonable explanation is an existence of salts in the original protein supplied by the producer. Namely, proteins are delivered with organic and inorganic additives such as sodium chloride and citrate. The additives probably crystallize upon drying, so the spikes observed in Figure 9 are probably salt crystals. Here it is worth mentioning that the height scales in Figure 8 and 9 are much different from the lateral scales. If the same scale is used for all three axes the spikes will shrink in height substantially. This hypothesis is supported by the XPS characterization of the samples during etching. The results summarized in Table 2 show a substantial increase in the concentration of inorganic materials (sodium in particular) after protein etching for a

short time. It is well known that reactive particles found in an oxygen plasma afterglow do not interact with inorganic salts, so the relative concentration increases after a layer of protein is removed.

The absence of chemical interaction between oxygen particles and inorganic material is probably the reason why the etching curves presented in Figure 4 are not linear. Pure organic materials like polymers are often etched at a constant rate as long as the processing parameters including the polymer temperature are kept constant. Such an observation was reported recently.^[21] The etching curves presented in Figure 4 can be approximated with linear dependence only near the origin, say for the first few 10 s of treatment, but definitely not for prolonged treatment times. Furthermore, some material also persists on the quartz sensors after very long treatment time. This observation, as well as the deviation from the linear dependence, is explained by the remaining inorganic additives. During the removal of the proteins the inorganic additives remain on the surface, thus screening the proteins. The effect is hardly noticeable at the beginning of the treatment when the proteins prevail, but it becomes increasingly important as more protein is removed. Finally, only the inorganic additives are left on the surface of quartz crystals. The deviation from linearity could be also explained by crosslinking reactions that give stronger bonds. During the treatment the as-synthesized material may become less and less reactive forming a kind of protective crust. Unfortunately, our experimental devices do not allow for distinguishing between this effect and the effects cause by inorganic additives. After prolonged treatment, gold peaks are observed in the XPS survey spectra as indicated in Figure 10. This figure represents two XPS survey spectra: the lower curve was obtained on a virgin Au-coated quartz crystal and the upper curve is for a crystal coated with fibrinogen and treated in the late afterglow for 2750 s. It is interesting that the virgin sample contains not only gold but also carbon as well as oxygen. Obviously, some impurities are adsorbed on the surface of such samples. Even more interesting is the upper curve which reveals a substantial amount of sodium which is not

balanced with chlorine. This discrepancy is well beyond the experimental error and is explained by the composition of the additives. Both sodium chloride and citrate are added. The chloride remains intact but citrate is oxidized by reactive oxygen particles, so after complete oxidation it is instead transformed into the sodium oxide. Taking into account this phenomenon, the oxygen concentration on the sample treated for a prolonged time (upper curve in Figure 10) is by far too large to be attributed to sodium oxide. The virtual discrepancy is explained if the results presented in Figure 11 are considered. This figure represents the high resolution XPS spectra of the Au4f peak. There is a huge difference in the chemical state of gold before and after treatment in the oxygen plasma late afterglow: before treatment gold is in a metallic phase, but after the treatment its oxidation state is changed to Au^{3+} due to surface oxidation. Such oxidation of gold in oxygen plasma had already been observed previously, and according to the binding energy it can be Al_2O_3 .^[34-37] Reactive oxygen particles in the late afterglow are obviously aggressive enough to form a thin gold oxide film on the sample surface.

Conclusion

Systematic measurements were performed in order to determine the etching rates for a couple of proteins mounted into the early and late afterglows of oxygen plasma. The etching rates were determined by measuring the resonant frequency of gold-plated quartz crystals. Commercially available fibrinogen and albumin samples were carefully deposited onto the crystals to form a film of uniform thickness. They were exposed to either the early or late afterglows of oxygen plasma created by a microwave discharge. The etching rates of several 0.1 nm s^{-1} were observed. Since the etching rate of polymers used in advanced medical instruments such as PET is at least 2 orders of magnitude lower,^[21] the technique is suitable for the removal of traces of blood proteins from such instruments after use in medical praxis. An attempt was made to explain the etching mechanism, and the hypothesis was developed

based on the thorough determination of the densities of atoms in the ground state, metastable molecules, and ozone molecules. The hypothesis assumes the synergistic effects of atoms and $O_2(a)$ molecules, while ozone plays a minor role, if any, in the etching of proteins with neutral reactive oxygen particles.

Acknowledgements: The authors acknowledge financial support from the Slovenian Research Agency throughout the project L7-4035 (Towards an ecologically benign alternative for the cleaning of delicate biomedical instruments). The authors acknowledge support from the Hungarian Science Foundation OTKA throughout K-104531 and the Hungarian - Slovenian Intergovernmental bilateral project TET-10-1-2011- 0638.

Received: ((will be filled in by the editorial staff)); Revised: ((will be filled in by the editorial staff)); Published online: ((please add journal code and manuscript number, e.g., DOI: 10.1002/ppap.201100001))

Keywords: afterglow plasma processes; etching kinetics; films; proteins; quartz crystal microbalance (QCM)

- [1] I.P. Limpscomb, A.K. Sihota, C.W. Keevil, *J. Clin. Microbiol.* **2006**, *44*, 3728.
- [2] D. Vujosevic, Z. Vratnica, A. Vesel, U. Cvelbar, M. Mozetic, A. Drenik, T. Mozetic, M. Klanjsek-Gunde, N. Hauptman, *Mater. Tehnol.* **2006**, *40*, 227.
- [3] D. Vujosevic, M. Mozetic, U. Cvelbar, N. Krstulovic, S. Milosevic, *J. Appl. Phys.* **2007**, *101*, 103305.
- [4] U. Cvelbar, D. Vujosevic, Z. Vratnica, M. Mozetic, *J. Phys. D: Appl. Phys.* **2006**, *39*, 3487.
- [5] O. Kylian, F. Rossi, *J. Phys. D: Appl. Phys.* **2009**, *42*, 085207.
- [6] U. Cvelbar, M. Mozetic, N. Hauptman, M. Klanjsek-Gunde, *J. Appl. Phys.* **2009**, *106*, 103303.
- [7] M. Moisan, J. Barbeau, S. Moreau, J. Pelletier, M. Tabrizian, L'H Yahia, *Int. J. Pharm.* **2001**, *226*, 1.
- [8] O. Kylian, H. Rauscher, L. Sirghi, F. Rossi, *J. Phys: Conf. Series* **2008**, *100*, 062017.
- [9] F. Rossi, O. Kylian, H. Rauscher, D. Gilliland, L. Sirghi, *Pure Appl. Chem.* **2008**, *80*, 1939.
- [10] O. Kylian, H. Rauscher, D. Gilliland, F. Bretagnol, F. Rossi, *J. Phys. D: Appl. Phys.* **2008**, *41*, 095201.
- [11] F. Rossi, O. Kylian, H. Rauscher, M. Hasiwa, D. Gilliland, *New J. Phys.* **2009**, *11*, 115017.
- [12] A.G. Whittaker, E.M. Graham, R.L. Baxter, A.C. Jones, P.R. Richardson, G. Meek, G.A. Campbell, A. Aitken, H.C. Baxter, *J. Hosp. Infect.* **2004**, *56*, 37.
- [13] D.M. Taylor, *J. Hosp. Infect.* **1999**, *43*, S69.
- [14] K. Fricke, H. Steffen, T. von Woedtke, K. Schröder, K.-D. Weltmann, *Plasma Process. Polym.* **2011**, *8*, 51.
- [15] K. Fricke, S. Reuter, D. Schröder, V. Schulz-von der Gathen, K.-D. Weltmann, T. von Woedtke, *IEEE Trans. Plasma Sci.* **2012**, *40*, 2900.

- [16] A. Vesel, T. Semenic, *Mater. Tehnol.* **2012**, *46*, 227.
- [17] M. Kunaver, M. Mozetic, M. Klanjsek Gunde, *Thin Solid Films* **2004**, *459*, 115.
- [18] V. Hody, T. Belmonte, C.D. Pintassilgo, F. Poncin-Epaillard, T. Czerwiec, G. Henrion, Y. Segui, J. Loureiro, *Plasma Chem. Plasma Process.* **2006**, *26*, 251.
- [19] T. Belmonte, C.D. Pintassilgo, T. Czerwiec, G. Henrion, V. Hody, J.M. Thiebaut, J. Loureiro, *Surf. Coat. Technol.* **2005**, *200*, 26.
- [20] V. Hody, T. Belmonte, T. Czerwiec, G. Henrion, J. M. Thiebaut, *Thin Solid Films* **2006**, *506-507*, 212.
- [21] A. Vesel, M. Kolar, A. Doliska, K. Stana-Kleinschek, M. Mozetic, *Surf. Interface Anal.* **2012**, *44/13*, 1565.
- [22] R. Zaplotnik, A. Vesel, M. Mozetic, *Sensors* **2012**, *12*, 3857.
- [23] G. Primc, R. Zaplotnik, A. Vesel, M. Mozetic, *AIP Advances* **2011**, *1*, 022129.
- [24] K. Kutasi, V. Guerra, P.A. Sá, *Plasma Sources Sci. Technol.* **2011**, *20*, 035006.
- [25] K. Kutasi, V. Guerra, P. Sa, *J. Phys. D: Appl. Phys.* **2010**, *43*, 175201.
- [26] V. Guerra, K. Kutasi, P.A. Sa, *Appl. Phys. Lett.* **2010**, *96*, 071503.
- [27] K. Kutasi, R. Zaplotnik, G. Primc, M. Mozetic, "Controlling the oxygen species density distributions in the flowing afterglow of O₂/Ar-O₂ surface-wave microwave discharges", submitted to *J. Phys. D. : Appl. Phys.*
- [28] A. Doliska, V. Ribitsch, K. Stana Kleinschek, S. Strnad, *Carbohydr. Polym.* **2013**, *93*, 246.
- [29] Human serum albumin, http://en.wikipedia.org/wiki/Human_serum_albumin, (accessed March, 2013).
- [30] S. Roy, A. Sun, C. Redman, *J. Biol. Chem.* **1996**, *271*, 24544.
- [31] R. Zaplotnik, D. Kreuh, A. Vesel, *Mater. Tehnol.* **2013**, *47/6*, 1.
- [32] W. Dal'Maz Silva, T. Belmonte, D. Duday, G. Frache, C. Noël, P. Choquet, H.-N. Migeon, A. M. Maliska, *Plasma Processes Polym.* **2012**, *9*, 207.

- [33] M.R. Wertheimer, A.C. Fozza, A. Höllander, *Nucl. Instrum. Meth. B* **1999**, *151*, 65.
- [34] B. Koslowski, H.-G. Boyen, C. Wilderotter, G. Kästle, P. Ziemann, R. Ahrenberg, P. Oelhafen, *Surf. Sci.* **2001**, *475*, 1-10.
- [35] H.-G. Boyen, G. Kästle, F. Weigl, B. Koslowski, C. Dietrich, P. Ziemann, J. P. Spatz, S. Riethmüller, C. Hartmann, M. Möller, G. Schmid, M. G. Garnier, P. Oelhafen, *Science* **2002**, *297*, 1533-1536.
- [36] K. Raiber, A. Terfort, C. Benndorf, N. Krings, H.-H. Strehblow, *Surf. Sci.* **2005**, *595*, 56-63.
- [37] A. Vesel, M. Kolar, A. Doliska, K. Stana-Kleinschek, M. Mozetic, *Surf. Interface Anal.* **2012**, *44*, 1565.

Figure captions:

Figure 1. Schematic diagram of the experimental system.

Figure 2. OES spectrum of glowing MW plasma.

Figure 3. Calculated densities of: a) $O_2(a)$ molecules and b) O_3 molecules along the afterglow chamber.

Figure 4. Thickness of the protein films *versus* treatment time in oxygen plasma early (EAG) and late (LAG) afterglows at a pressure of 50 Pa.

Figure 5. Maximum etching rates of the proteins fibrinogen and HSA in early (EAG) and late (LAG) afterglows *versus* pressure.

Figure 6. Ratio O/C and N/C of: a) fibrinogen and b) albumin *versus* time after etching in early and late oxygen afterglows (determined from XPS measurements).

Figure 7. Comparison of XPS C1s spectra of as-deposited (reference) and plasma-etched albumin and fibrinogen in early and late oxygen afterglows.

Figure 8. AFM images of albumin *versus* etching time in early and late afterglows measured on $2 \times 2 \mu\text{m}^2$.

Figure 9. AFM images of fibrinogen *versus* etching time in early and late afterglows measured on $5 \times 5 \mu\text{m}^2$.

Figure 10. XPS survey spectra for a virgin Au-coated quartz crystal (lower curve) and a crystal coated with fibrinogen and treated in a late afterglow for 2750 s (upper curve).

Figure 11. High resolution gold peaks for a virgin Au-coated quartz crystal (lower curve) and a crystal coated with fibrinogen and treated in a late afterglow for 2750 s (upper curve).

Figure 12. Product of the densities of atoms O (3P) and molecules in the first excited state $O_2(a)$.

Table captions:

Table 1. Measured density of neutral oxygen atoms $O(^3P)$ and calculated density of $O_2(a)$ and O_3 molecules in early and late afterglows of oxygen plasma.

Table 2. XPS surface composition of fibrinogen and albumin versus time after etching in early and late oxygen afterglows for different periods (at.%).

For Peer Review

Table 1. Measured density of neutral oxygen atoms $O(^3P)$ and calculated density of $O_2(a)$ and O_3 molecules in early and late afterglows of oxygen plasma.

Pressure [Pa]	LAG			EAG		
	$O(^3P)$ [m^{-3}]	$O_2(a)$ [m^{-3}]	O_3 [m^{-3}]	$O(^3P)$ [m^{-3}]	$O_2(a)$ [m^{-3}]	O_3 [m^{-3}]
50	7.0×10^{20}	0.8×10^{21}	0.3×10^{19}	13.5×10^{20}	1.0×10^{21}	0.02×10^{19}
100	6.0×10^{20}	2.3×10^{21}	0.8×10^{19}	11.5×10^{20}	2.6×10^{21}	0.04×10^{19}
150	5.0×10^{20}	4.0×10^{21}	2.0×10^{19}	9.5×10^{20}	4.4×10^{21}	0.1×10^{19}
200	4.0×10^{20}	5.5×10^{21}	3.5×10^{19}	7.5×10^{20}	6.0×10^{21}	0.2×10^{19}
300	3.0×10^{20}	8.5×10^{21}	8.0×10^{19}	6.0×10^{20}	9.0×10^{21}	0.7×10^{19}
400	2.5×10^{20}	11.0×10^{21}	14.0×10^{19}	5.0×10^{20}	12.0×10^{21}	2.1×10^{19}

Table 2. XPS surface composition of fibrinogen and albumin versus time after etching in early and late oxygen afterglows for different periods (at.%).

sample	C	O	N	Na	Cl	S	P	O/C	N/C
ALB powder as-received	65.7	17.8	15.2	0.5		0.8			
ALB, as-deposited	74.5	14.5	10.0			0.4	0.6	0.2	0.1
ALB, EAG, 90 s	44.9	33.1	13.6	7.4		0.6	0.3	0.7	0.3
ALB, EAG, 180 s	43.3	34.8	14.5	5.7		1.3	0.4	0.8	0.3
ALB, LAG, 300 s	45.6	33.3	13.6	6.4		0.6	0.3	0.7	0.3
ALB, LAG, 600 s	44.9	33.6	14.6	4.6		0.9	0.4	0.7	0.3
FIB powder as-received	40.4	30.0	2.0	19.5	8.1				
FIB, as-deposited	69.7	15.9	12.2	1.4	0.9			0.2	0.2
FIB, EAG, 30 s	51.3	26.7	13.2	6.9	1.8			0.5	0.3
FIB, EAG, 60 s	48.5	29.7	11.1	9.1	1.2			0.6	0.2
FIB, EAG, 150 s	42.4	28.9	13.2	8.3	2.4			0.7	0.3
FIB, LAG, 100 s	48.1	28.2	13.9	7.8	1.7			0.6	0.3
FIB, LAG, 200 s	48.4	27.7	13.7	7.6	2.1			0.6	0.3

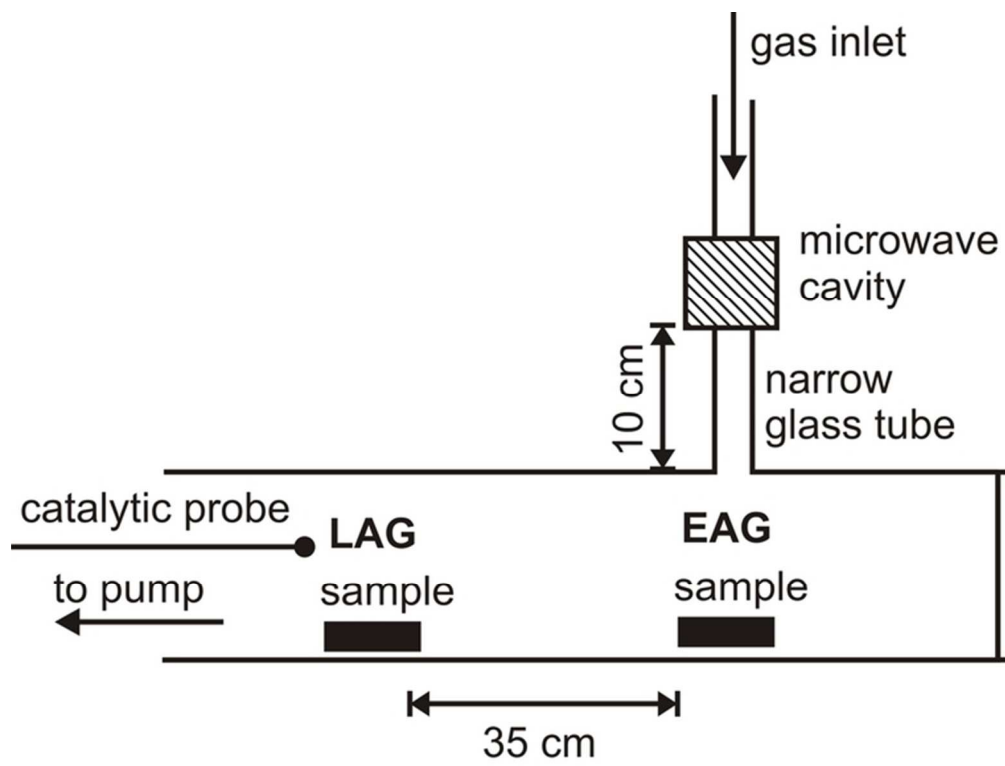


Figure 1. Schematic diagram of the experimental system.
64x49mm (300 x 300 DPI)

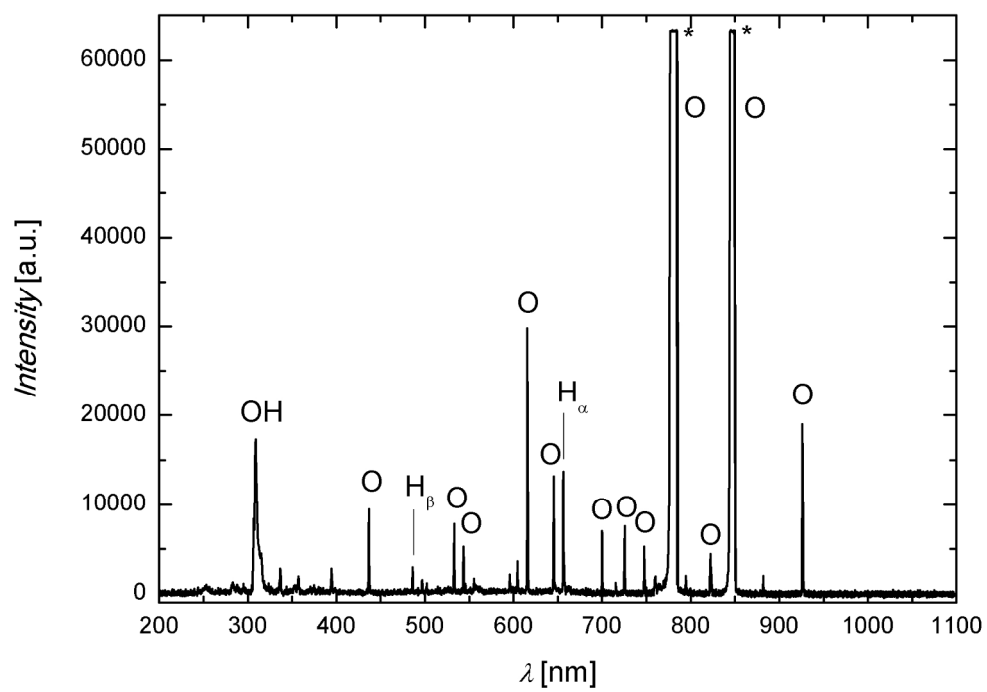


Figure 2. OES spectrum of glowing MW plasma.
184x134mm (300 x 300 DPI)

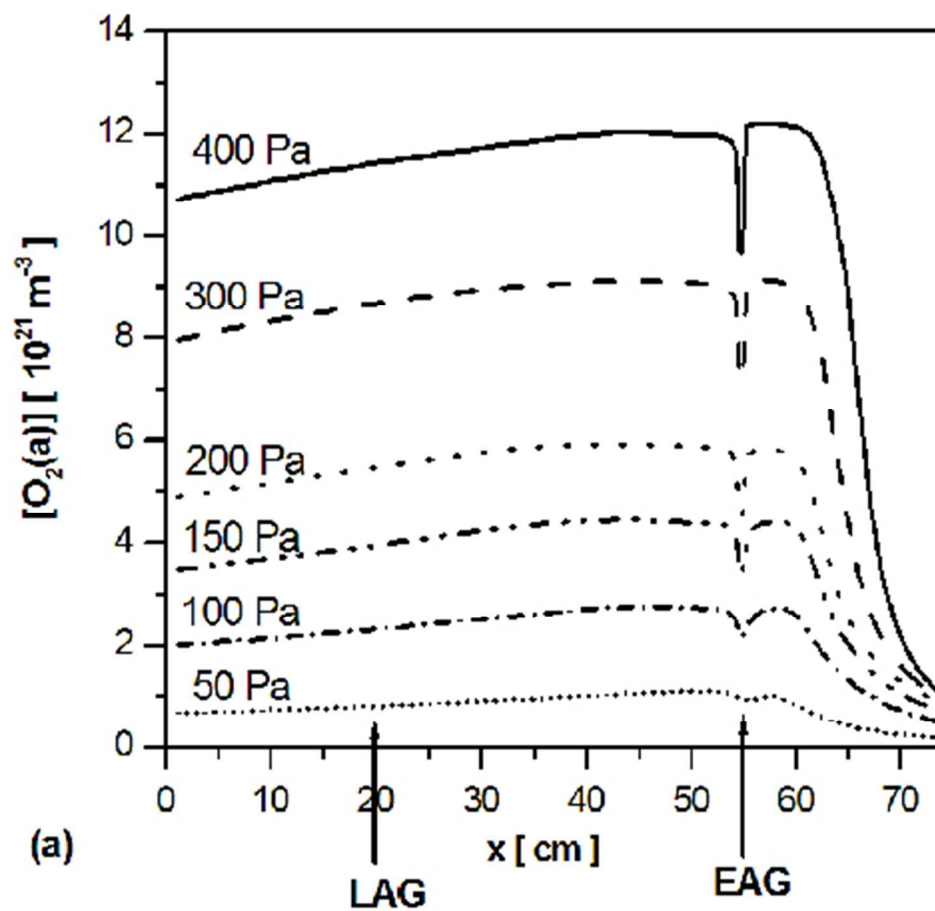


Figure 3. Calculated densities of: a) $O_2(a)$ molecules and b) O_3 molecules along the afterglow chamber. 85x79mm (150 x 150 DPI)

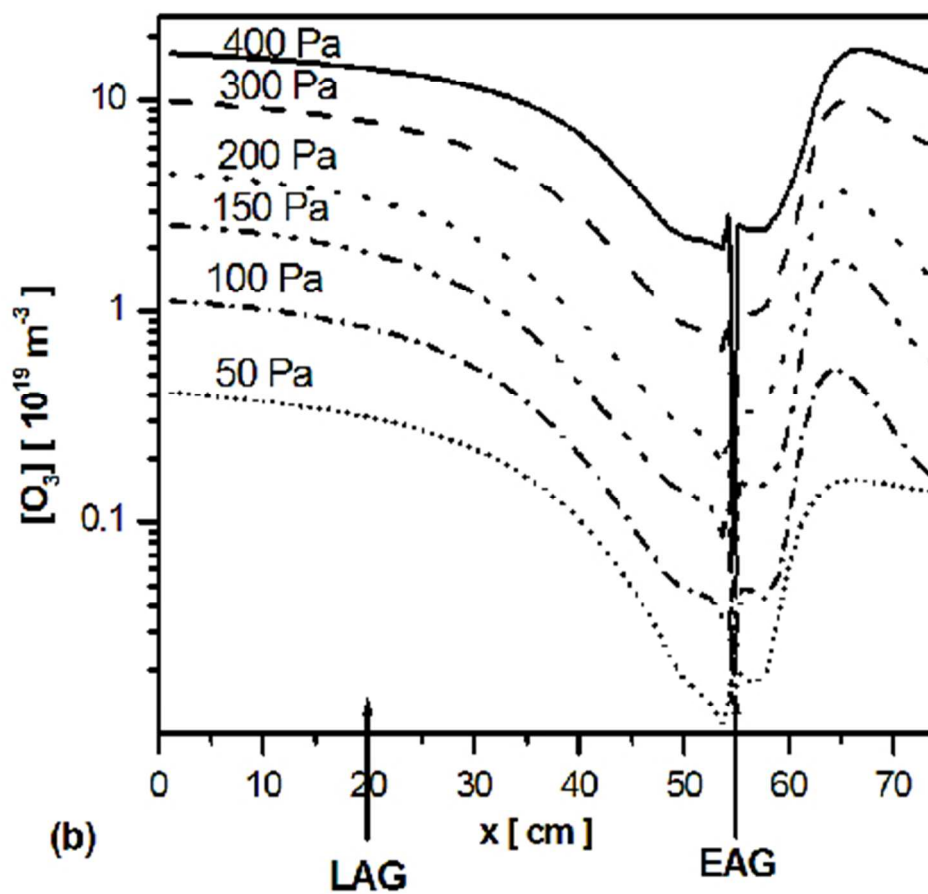


Figure 3. Calculated densities of: a) O₂(a) molecules and b) O₃ molecules along the afterglow chamber.
85x79mm (150 x 150 DPI)

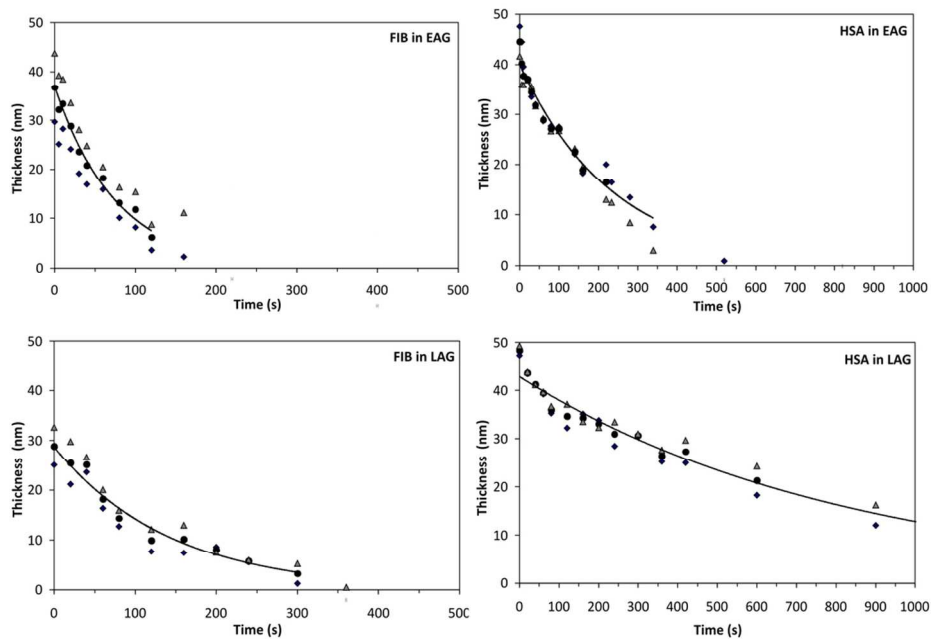


Figure 4. Thickness of the protein films versus treatment time in oxygen plasma early (EAG) and late (LAG) afterglows at a pressure of 50 Pa.
103x67mm (300 x 300 DPI)

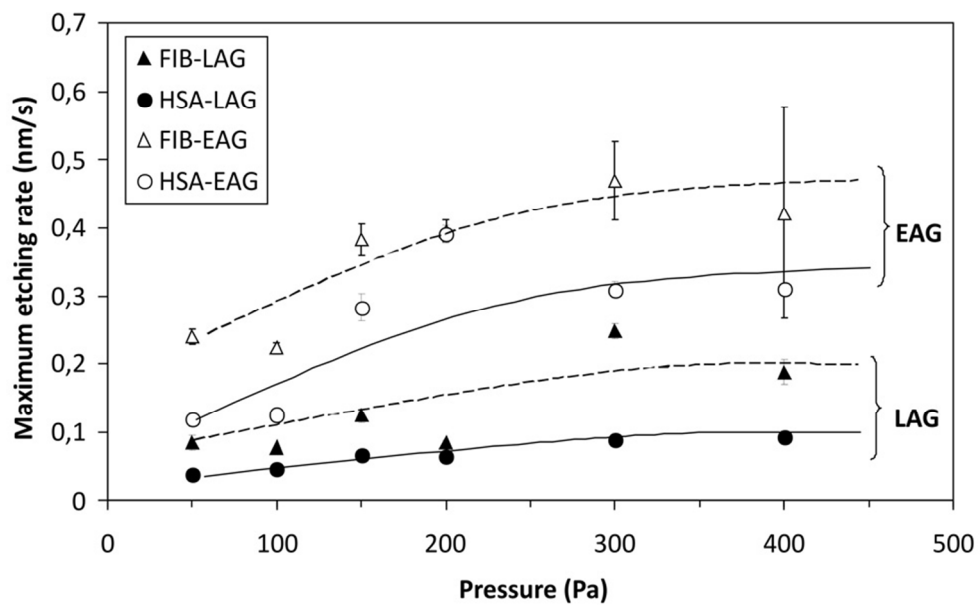


Figure 5. Maximum etching rates of the proteins fibrinogen and HSA in early (EAG) and late (LAG) afterglows versus pressure.
85x51mm (300 x 300 DPI)

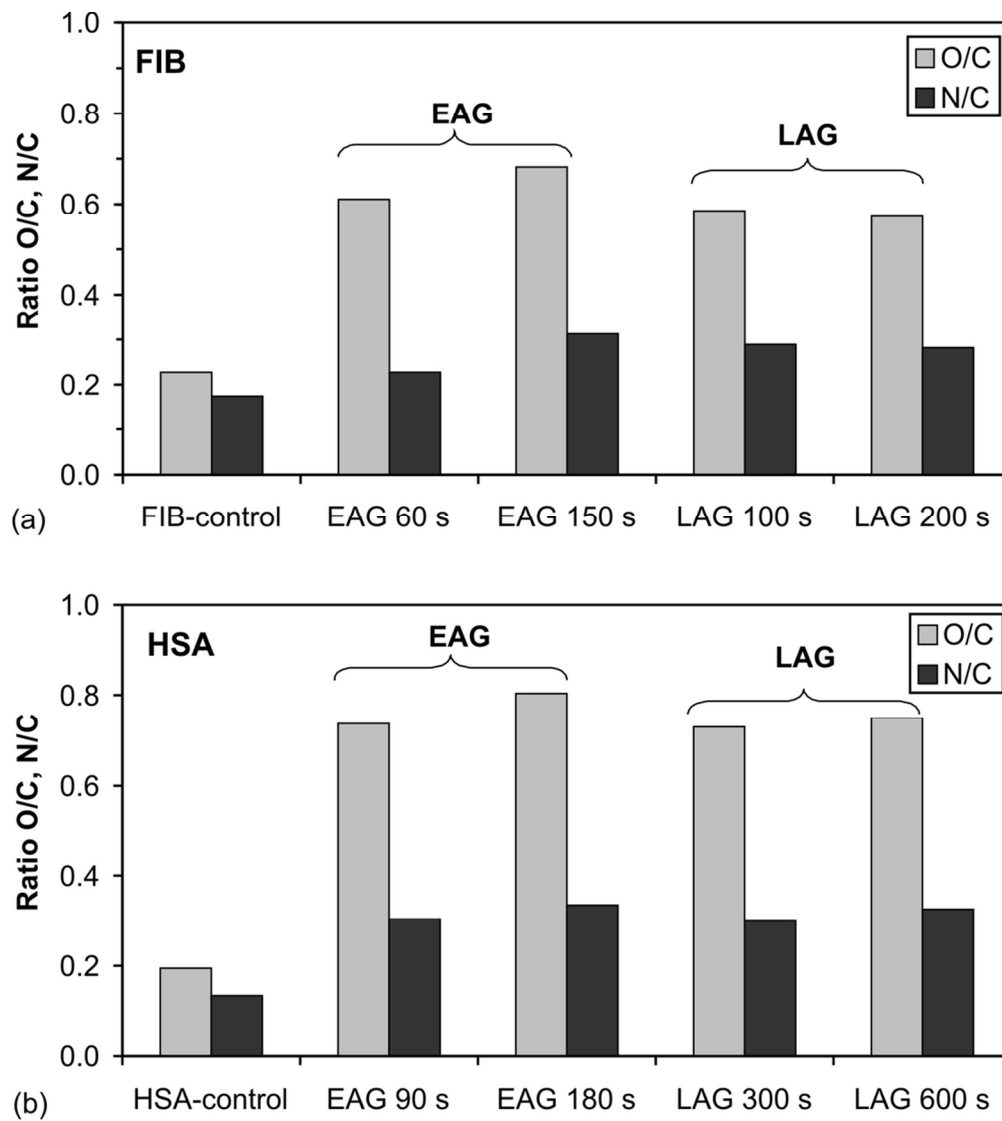


Figure 6. Ratio O/C and N/C of: a) fibrinogen and b) albumin versus time after etching in early and late oxygen afterglows (determined from XPS measurements).
93x103mm (300 x 300 DPI)

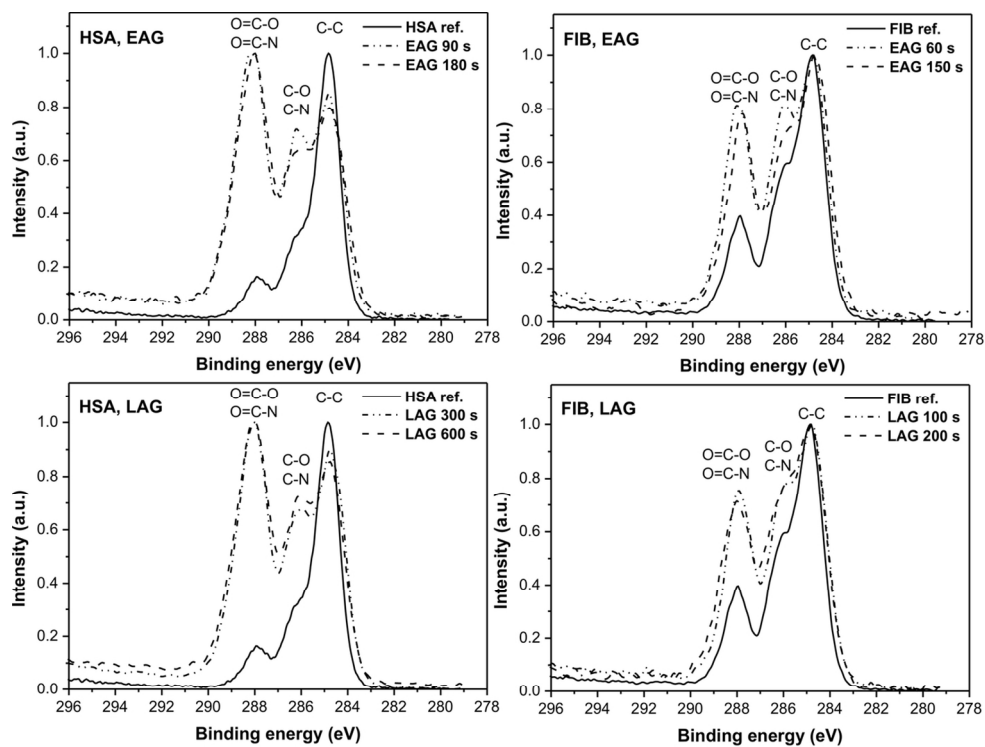


Figure 7. Comparison of XPS C1s spectra of as-deposited (reference) and plasma-etched albumin and fibrinogen in early and late oxygen afterglows.
122x94mm (300 x 300 DPI)

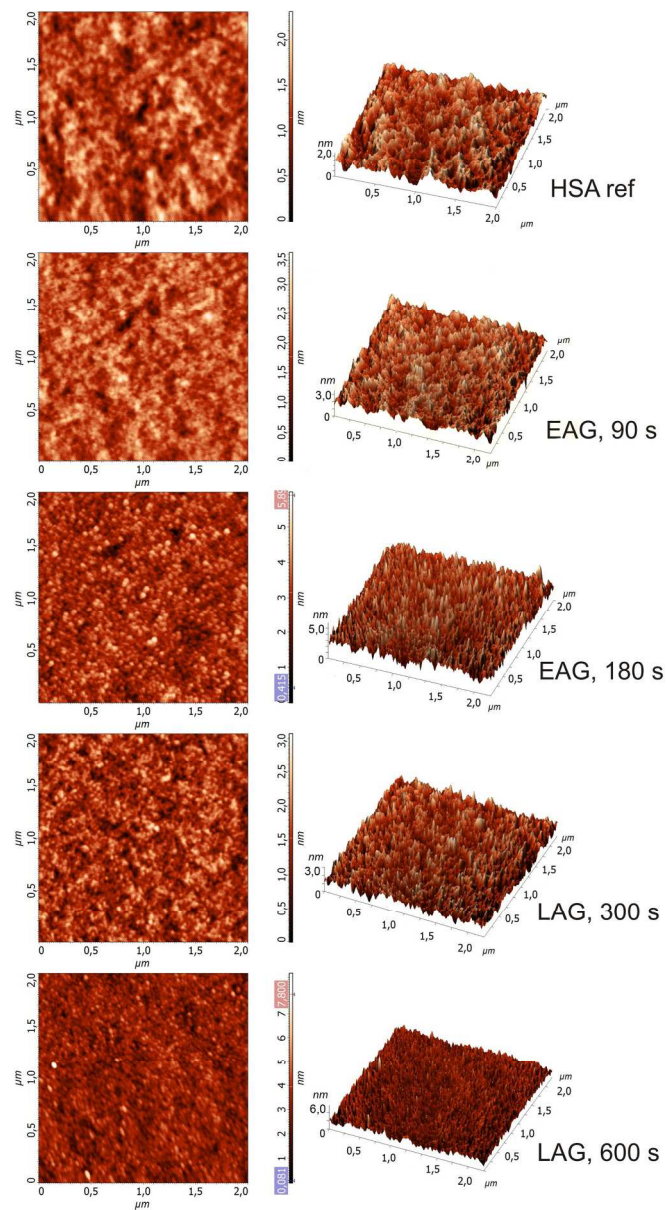


Figure 8. AFM images of albumin versus etching time in early and late afterglows measured on $2 \times 2 \mu\text{m}^2$. 145x248mm (300 x 300 DPI)

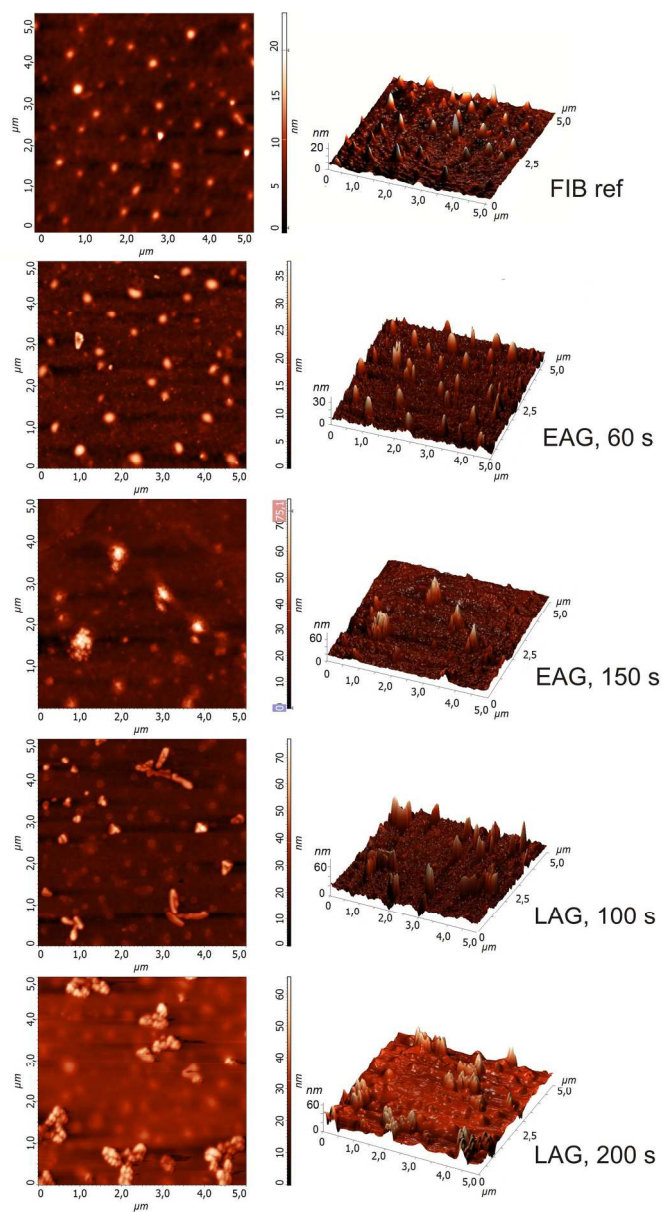


Figure 9. AFM images of fibrinogen versus etching time in early and late afterglows measured on $5 \times 5 \mu\text{m}^2$. 146x251mm (300 x 300 DPI)

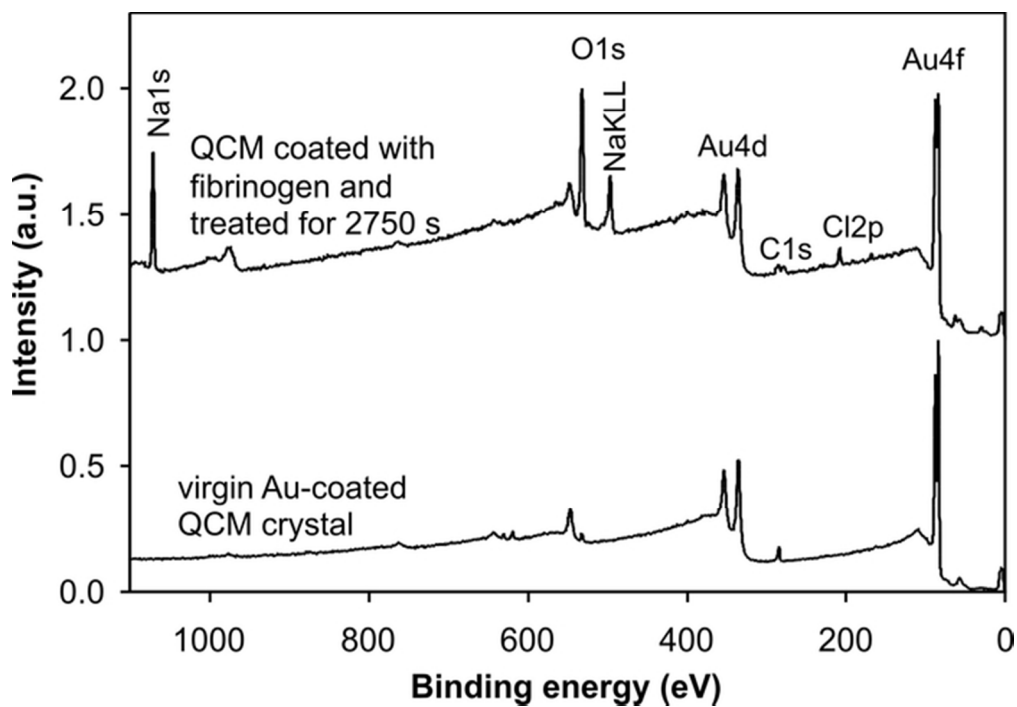


Figure 10. XPS survey spectra for a virgin Au-coated quartz crystal (lower curve) and a crystal coated with fibrinogen and treated in a late afterglow for 2750 s (upper curve).
58x40mm (300 x 300 DPI)

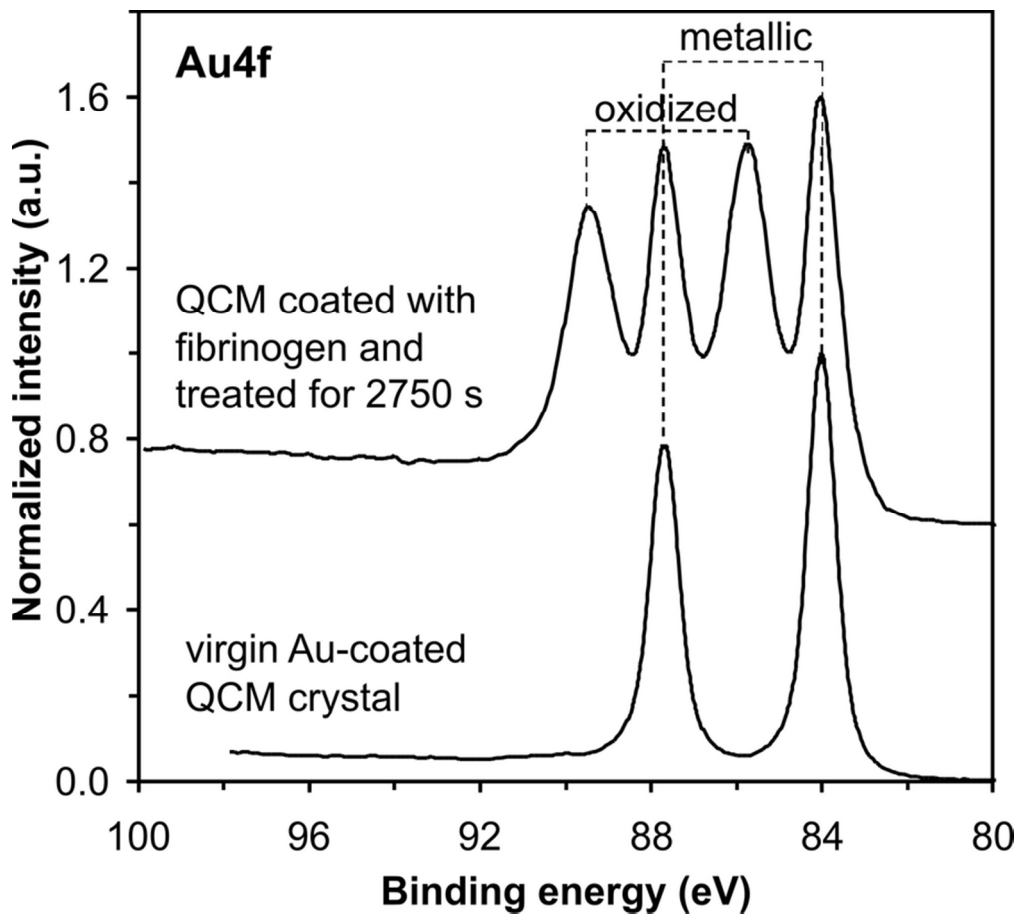


Figure 11. High resolution gold peaks for a virgin Au-coated quartz crystal (lower curve) and a crystal coated with fibrinogen and treated in a late afterglow for 2750 s (upper curve).

76x69mm (300 x 300 DPI)

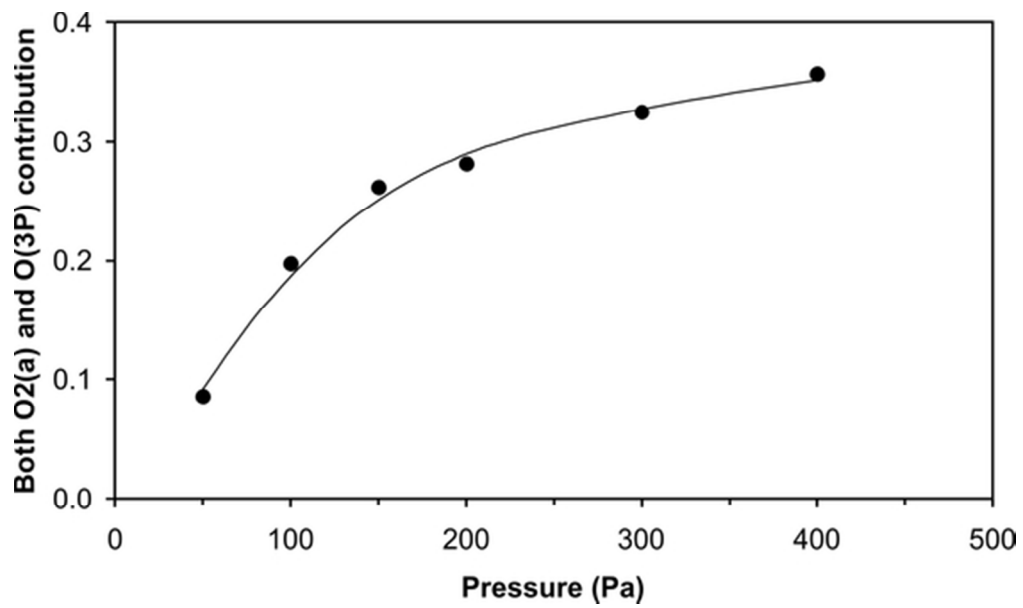


Figure 12. Product of the densities of atoms O (3P) and molecules in the first excited state O₂(a).
50x29mm (300 x 300 DPI)